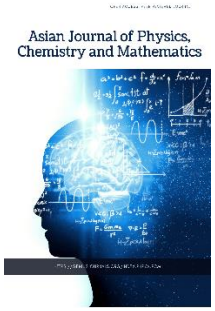

A recent study of the structural properties between of Mn-Zn-Fe_2O_4 and Mn-Zn-Fe_2O_4 /TiO_2 nanocomposite

Muthana El ttayef Abbas[1],

Iraq, University of Diyala, College of Science, Department of physics
*Corresponding author
E-mail: zenaalbana@yahoo.com ; ffamu55@gmail.com

Zena Mohammed Ali abbas[1]

Iraq, University of Diyala, College of Science, Department of physics
*Corresponding author
E-mail: zenaalbana@yahoo.com ; ffamu55@gmail.com

ABSTRACT

In order for the nanomaterials to be utilized, it is vital to be able to control the structural properties of the Mn-Zn-ferrites nanoparticles (NPs) by sol-gel and Mn-Zn-ferrites /TiO_2 nanocomposite (NC) generated by sol – gel method at 650, 750, and 850 ^oC. An examination into the possibility of producing the Mn-Zn-ferrites by sol-gel and Mn-Zn-ferrites /TiO_2 (NC) as prospective structure-tunable nanomaterials is described in this report. X-ray diffraction (XRD), field emission-scanning electron microscopy (FE-SEM), and Fourier-transform infrared (FTIR) spectroscopy were used to characterize the structural properties of the Mn-Zn-ferrites by sol-gel and Mn-Zn-ferrites /TiO_2 (NC). They were 27 to 30 nm in size with a cubic structure, while the Mn-Zn-ferrites /TiO_2 (NC) were 10 to 30 nm in size with a cubic structure. FE-SEM images showed the synthesized the Mn-Zn-ferrites and the Mn-Zn-ferrites /TiO_2 (NC) had a nanoparticle-like structure with a particle size of 27.77, to 72.04 nm. The strong FT-IR absorption peaks at 500 and 600 cm^{-1} represented an Fe-O, Mn-O, and Zn-O vibration band and 1667 cm^{-1} represented an TiO_2 for the Mn-Zn-ferrites and the Mn-Zn-ferrites /TiO_2 (NC), respectively.

Keywords: Mn-Zn-ferrites; Mn-Zn-ferrites /TiO_2 NC: Structural properties; Sol-gel method.

1. Introduction

A key component of nanomedicine and nanobiotechnology is the use of nanomaterials. Antibiotic-resistant microorganisms may be able to benefit from this new strategy [1]. Because of their unique physical, chemical, mechanical, and magnetic properties, nanoparticles (NPs) have been shown in multiple studies to be therapeutic agents for treating infections caused by bacteria. As a result, new bactericidal agents are being developed using NPs in clinical settings [2-3]. An efficient prevention of bacterial growth can be achieved by using nanoscale materials that can penetrate into bacterial cells and produce deadly oxygen ion radicals that damage the cell membranes of germs [4-7]. Using spinel-structured ferrite nanoparticles in magnetic resonance imaging, magnetic storage devices, biotechnology, electronic devices, magnetic medication delivery, and other fields has made a significant influence on science researchers [8-10]. For many applications, magnetic nanoparticles require super-paramagnetic properties at room temperature because of their huge surface-to-volume ratio [11-14].

$MnFe_2O_4$ and nanoparticles have the highest surface area, the highest saturation magnetization, the highest mechanical hardness, and the best chemical stability of all spinel ferrites [15]. It has been found in the literature that manganese ferrite nanoparticles may be manufactured using a variety of processes, including classic ceramic methods, oxalate method, sol–gel method, chemical co-precipitation and mechanical ball milling [16]. There are numerous uses for the sol–gel process, which is one of the most widely used procedures. Scientists used this method to create some of the world's lightest materials and some of the toughest ceramics. The spin or dip coating of thin films on a substrate using the sol–gel technique has a wide range of applications. It's possible to make glass objects with unique features that can't be achieved any other way. The sol–gel method has used a variety of surfactants up to this point, but there is no information on the effects of WF and PF as surfactants. For the production of manganese ferrite, WF and PF were employed as surfactants. A and B samples of $MnFe_2O_4$ and Mn-Zn-Fe_2O_4 /TiO_2 were studied for their structural, morphological properties (XRD analysis, FT-IR spectroscopy, Filed emission scanning electron microscopy (FE-SEM)). Particle size and shape, morphology, and chemical composition all play important roles in determining the samples' physical qualities, however these factors cannot always be controlled during the nanoparticle production process [16]. For Manganese-Zinc-Ferrite (Mn-Zn-Fe_2O_4) nanocomposite prepared through ceramic methods like sol-gel, the composition, cationic distribution and thermal behavior of oxygen are very often in-ter related, leading to an important dependence of the mi-cross structure and therefore its physical properties, with the atmosphere and heat treatment temperatures [17].

Despite this, sol-gel synthesis is a viable option with significant economic and technological advantages as well as excellent reproducibility, and it can produce monodisperse nanoparticles with good crystallinity when the synthesis process is conducted with the right control [18-19]. By using XRD analysis (XRD-6000/Japan), the (Mn-Zn-Fe_2O_4) nanocomposite was characterized and the findings were compared to the JCPDS card data (Joint Committee on Powder Diffraction Standards). In Iraq's Nanotechnology and Advanced Materials/Materials Research Department/Ministry of Science and Technology, XRD measurements have examined the orientation of (Mn-Zn-Fe_2O_4) nanocomposite grown samples. In Iran-Mashhad, "(Tescan Mira3 FE-SEM-Czechia)" employed FE-SEM to analyze the morphology and particle size of (Mn-Zn-Fe_2O_4). Fourier transformed infrared spectrum (FTIR) was utilized to study the functions group and vibrations modes utilizing a potassium bromide (KBr) beam splitter and a mid IR triglycine sulfate (TGC) detector for the polarized IR reflectance. The magnetic characteristics were examined utilizing an MPMS XL, Quantum Design SQUID magnetometer by VSM.

2. Experimental work

2.1 The materials used

The materials used in the preparation of the ferrite compound by sol-gel auto combustion method are listed in table 1 with their full description.

Table (1): The chemical materials and their properties

Compounds	Chemical formula	Mol. mass (g mol-1)	Purity %	Origin
Titanium oxide	TiO_2	79.87	99.00	USA
Iron (III) nitrate	$Fe(NO_3)_{3.9}H_2O$	404.00	97.00	India
Citric acid	$C_6H_8O_7.H_2O$	210.14	99.00	USA

Ammonia solution	NH3	30.01	25	India
Zinc nitrate	$Zn(NO_3)_{2.6}H_2O$	297.37	98.0	India
Manganese(II) nitrate	$Mn(NO_3)_{2.4}H_2O$	250.93	98.0	USA

2.2 Preparation method of the Mn-Zn-ferrites and Mn-Zn-ferrites /TiO_2 nanocomposite

All metal nitrate and citric acid were dissolved in 15 ml of distilled water. All of them are combined in a glass beaker to form a complete solution, which is thoroughly mixed at room temperature with a magnetic stirrer at high speeds for a short time until the solution becomes smooth and slimy red-colored, as shown in figure (1a). Ammonia solution was steadily injected into the mixed solution in the form of drips with continual stirring to regulate its pH until it reached the value of (7), resulting in a dark brown tint as seen in the picture (1 b). To achieve homogeneity, stir the components together for half an hour at room temperature. Gradually raise the temperature until it reaches 90 °C, stirring constantly until the gel form is reached. The size of the solution in the beaker glass be less with high viscosity, and after (30 minutes), the solution viscosity is very high, resulting in the beginning of gel formation on the surface of the solution, particularly in the middle, and then all of the solution turns to gel, and even at this point, the solution is still on the magnetic stirrer and temperature (90 C), as shown in Figure (1 c). The temperature decreases to room temperature after the solution turns to gel, the gel dries, and the hue changes to dark brown. Where the weight of the gel is placed in a glass beaker using a sensitive balance, and then placed in the oven at 150°C for three hours to dry the gel and reduce its weight as shown in Figure (1d). After evaporating some of the material and raising the temperature of the dried gel to (250°C), the dry gel began to change shape and become convex in the middle of the glass beaker after 15 minutes, as illustrated in figure (1 e). After combustion, the dried gel turns into a fine powder with a dark gray hue, signaling the start of the creation of high purity ferrite, as illustrated in the picture (1f-g). The spinel was then calcined for three hours at temperatures of (650,750, and 850 C) to improve crystallization and homogenous action distribution, and then ground to produce $Zn_xMn_{1-x}Fe_2O_4$ ferrite Nano powders. Using the traditional ceramic method, titanium dioxide is mixed with zinc-manganese ferrite in different quantities at 500°C.

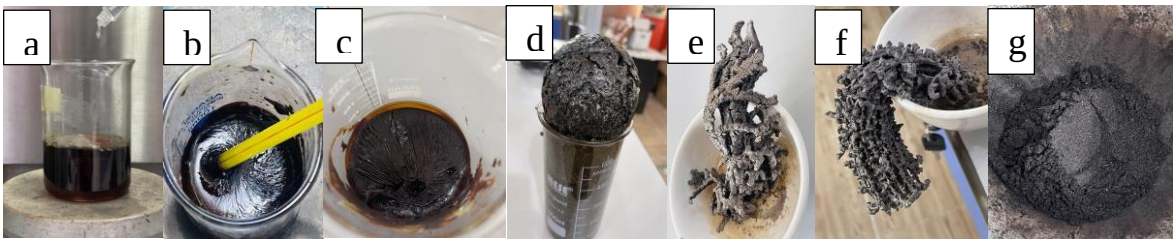

Figure (1): Photograph of (a) nitrates-citrate solution, (b) The solution after the Adding of ammonia, (c) dry gel, (d) Dry bulk temperature of 150C, (e) Dry bulk temperature of 250C and (f-g) auto combustion and become Nano powder ferrite.

2.3 Calcinations and Pellet Formation

The resulting powder is placed in a ceramic pot and then roasted at 650, 750, 850 °C for two hours to remove reaction residues such as water or carbon dioxide molecules from combustion, resulting in the necessary ferrite powder. Then 0.5 g of burnt samples and samples that were calcined at 650, 750 and 850 were taken and five drops of PVA were added as a binder to be pressed into round pellets 1 cm in diameter and 3 mm thick. This is achieved by pressing 500Pa for five minutes

with a hydraulic press using the dry-press method, then sintering at 400, 600 and 800 for 2 hours to thicken the samples and allow them to cool slowly naturally to check their dielectric properties, as shown in figure (2).

Figure (2): Transformation of powder to compact sample.

3. Result and discussion

3.1 XRD of the Mn-Zn-ferrites and Mn-Zn-ferrites /TiO_2 nanocomposite

From figure 3 observed that at the concentration of zinc metal (x=0.45), a pure single-phase cubic spinel $Zn_xMn_{1-x}Fe_2O_4$ structure was obtained with space group (Fd-3m no. 277), crystal dimensions (a = b = c = 8.438 A˚) and crystal angles (α = β = γ = 90˚), agreed with the standard data (JCPDS 98-017-0912) as shown in figure 3. The XRD patterns at high calcination temperatures 750 and 850 ^oC demonstrated that the distinct structural stability of obtained $Zn_xMn_{1-x}Fe_2O_4$ during the calcination process leads to crystalline growth in the same cubic $Zn_xMn_{1-x}Fe_2O_4$ structure with a high purity phase, no other impurities peaks were detected, this is an indication that all the reactant metal ions entered into the cubic $Zn_xMn_{1-x}Fe_2O_4$ structure at the concentration of zinc metal (x=0.45) [20]. The lattice constant value an of pure cubic $Zn_xMn_{1-x}Fe_2O_4$ ferrite nanocomposite is reduced when Zn metal added which can be explained on the basis of cations distribution, as a result of replacing larger ionic radii of Mn^{+2} cations (0.082 nm) by smaller ionic radii of Zn^{+2} cations (0.074 nm) [21-22]. In order to investigate the synthesized $Zn_{0.45}Mn_{0.55}Fe_2O_4$ ferrite nanocomposite mixed with different content of TiO_2 nanoparticles and calcined at 500 ^oC, Figure 4 presents the XRD patterns of pure TiO_2 nanoparticles and $Zn_{0.45}Mn_{0.55}Fe_2O_4$ mixed with different ratios (20, 30, 40, 50 and 60%) of TiO_2 nanoparticles. All the obtained peaks of $Zn_{0.45}Mn_{0.55}Fe_2O_4/TiO_2$ (40:60%) nanocomposite are assigned to the characteristic peaks of two main phases which are cubic spinel $Zn_{0.45}Mn_{0.55}Fe_2O_4$ phase (marked with red stars) (98-017-0912) and tetragonal TiO_2 phase (Anatase) (marked with blue stars) with space group (I41/amd no.141) (98-015-4609), in addition to little cubic $MnFe_2O_4$ phase (marked with black stars) (98-003-0237). The peak intensity proportion of tetragonal TiO_2 (011) to $Zn_{0.45}Mn_{0.55}Fe_2O_4$ (113) obviously increased with increase the mixed TiO_2 content in the structure of $Zn_{0.45}Mn_{0.55}Fe_2O_4/TiO_2$ nanocomposites

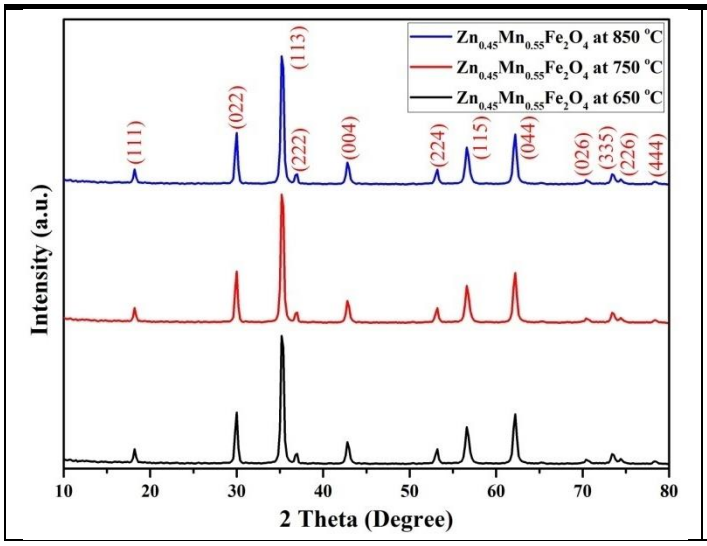

Figure 3 XRD patterns of $Zn_{0.45}Mn_{0.55}Fe_2O_4$ ferrite nanocomposites at different calcination temperatures (650, 750, 850 ˚C).

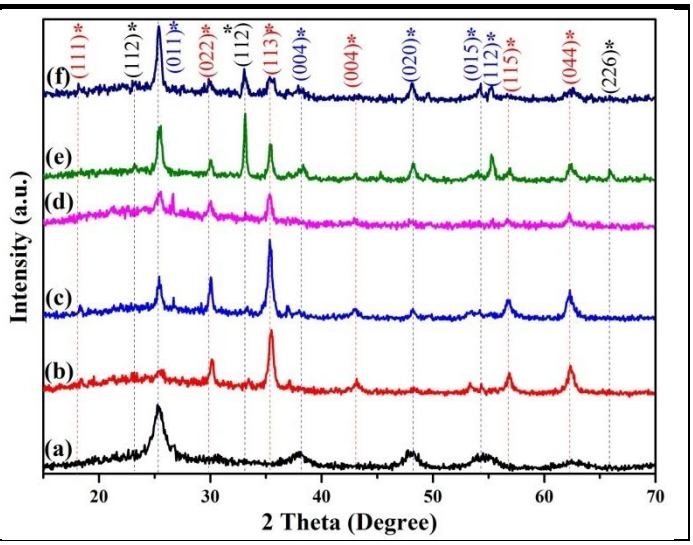

Figure 4 XRD patterns of (a) pure TiO_2, (b), (c), (d), (e) and (f) are $Zn_{0.45}Mn_{0.55}Fe_2O_4$ mixed with different ratios of TiO_2 (20, 30, 40, 50 and 60%) respectively.

The crystalline size of synthesized $Zn_{0.45}Mn_{0.55}Fe_2O_4$ at different calcination temperature was calculated using the Debye–Scherrer's equation, to be (27.99, 29.07 and 30.77 nm) at the temperature (650, 750 and 850 °C) respectively, as shown in table 2, 3, which presents the XRD calculations of synthesized $Zn_xMn_{1-x}Fe_2O_4$. Observed that the crystalline size slightly increased with raising the calcination temperature and the zinc content which is the common behavior of all synthesized material, attributed to the crystal growth with increase the calcination temperature and the zinc content, and this is corresponded with the measured XRD patterns where the intensity of the most intense peak (113) of pure $Zn_{0.45}Mn_{0.55}Fe_2O_4$ is significantly increases and the pattern appears narrower with the increasing of Zn content [2**Error! Bookmark not defined.**]. On other side, the crystalline size of TiO_2 nanoparticles is (10.76 nm).

Table 2 XRD calculations of $Zn_xMn_{1-x}Fe_2O_4$ with different content of zinc metal (x=0, 0.15, 0.25, 0.35 and 0.45) at different calcination temperatures.

Material	Temp. °C	2Θ (deg) Practical	2Θ (deg) Standard	FWHM (deg)	Crystalline size (nm)	d_{hkl} (°A) Practical	d_{hkl} (°A) Standard	(hkl)
$Zn_{0.45}Mn_{0.5}Fe_2O_4$	650	35.27	35.24	0.2704	27.99	2.5443	2.5441	(113)
	750	35.27	35.24	0.2604	29.07	2.5443	2.5441	(113)
	850	35.27	35.24	0.2462	30.77	2.5376	2.5441	(113)

Table 3 XRD calculations of $Zn_{0.45}Mn_{0.55}Fe_2O_4$ mixed with different content of TiO_2.

Material	TiO_2 content %	2Θ (deg) Practical	2Θ (deg) Standard	FWHM (deg)	Crystalline size (nm)	d_{hkl} (°A) Practical	d_{hkl} (°A) Standard	(hkl)
$Zn_{0.45}Mn_{0.55}Fe_2O_4/TiO_2$	20	35.27	35.24	0.2462	-	2.5376	2.5441	(113)
$Zn_{0.45}Mn_{0.55}Fe_2O_4/Ti$	30	35.26	35.24	0.295	-	2.5347	2.5441	(113

O_2				4				)
$Zn_{0.45}Mn_{0.55}Fe_2O_4/TiO_2$	40	35.28	35.24	0.2952	-	2.5401	2.5441	(113)
$Zn_{0.45}Mn_{0.55}Fe_2O_4/TiO_2$	50	25.45	25.42	0.3936	-	3.4992	3.5001	(011)
$Zn_{0.45}Mn_{0.55}Fe_2O_4/TiO_2$	60	25.35	25.42	0.2952	-	3.5129	3.5001	(011)
TiO_2	100	25.39	25.42	0.7200	10.76	3.5107	3.5001	(011)

3.2 FE-SEM of the Mn-Zn-ferrites and Mn-Zn-ferrites /TiO2 nanocomposite

The particle size got larger when the calcination temperature was raised, as shown in the FE-SEM image. FE-SEM images of manganese ferrite nanoparticles after calcination at (650, 750, and 850) ^oC are shown in Figures 5 (A-C) At 650 ^oC, spherical ferrite particles agglomerated and separated significantly. At greater calcination temperatures, larger spherical and elongated particles were observed.

As shown in Figure 6 (T1-T5), FE-SEM images were utilized to examine the surface morphology and particle size of $Zn_{0.45}Mn_{0.55}Fe_2O_4/TiO_2$ nanocomposites calcined at 500 °C (T1, T2, T3, T4 and T5) All of the specimens contain a compact order of homogenous nanoparticles with a spherical form and polyhedral particles. The estimated diameters of $Zn_{0.45}Mn_{0.55}Fe_2O_4/TiO_2$ nanocomposites for calcined samples at 500 with relatively well-crystallized grains and average particle size less than 27.77, 43.60, 61.51, 47.29 and 72.04 nm respectively calculated by Image J Software. All data agree relatively well with the XRD results. We also note the coalescence of adjacent grains with each other due to the increase in the concentration of TiO_2.

The particle size measured using FE-SEM micrographs is larger than the XRD data estimates. The XRD method is responsible for the molecular structural disruption and lattice strain generated by differing ionic radii and/or nanoparticle collection. As a result, it has a more stringent requirement, which leads to lower sizes [24].

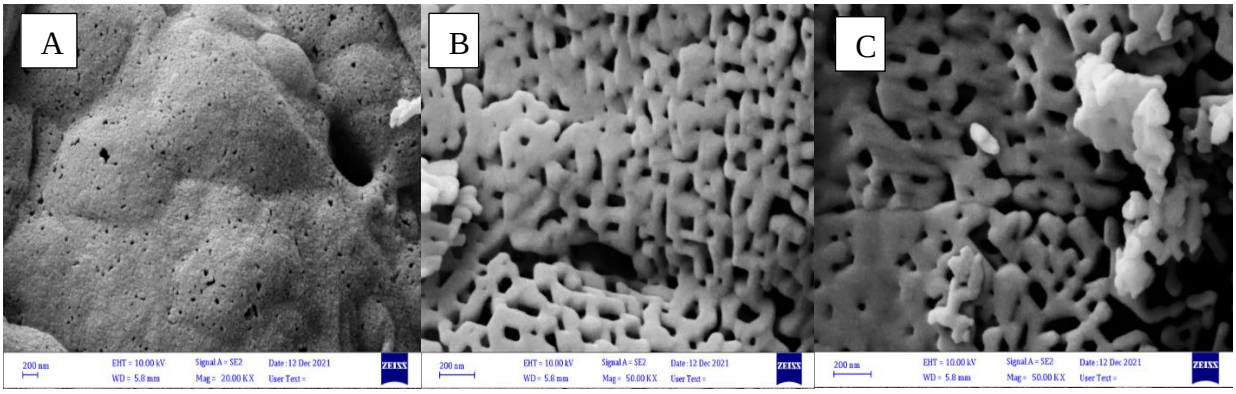

Figure (5): FE-SEM micrographs of $Zn_{0.45}$ $Mn_{0.55}$ Fe_2O_4 Nano ferrites for (A) calcined specimen at 650 ℃ (B) at 750 ℃ and (C) at 850 ˚C.

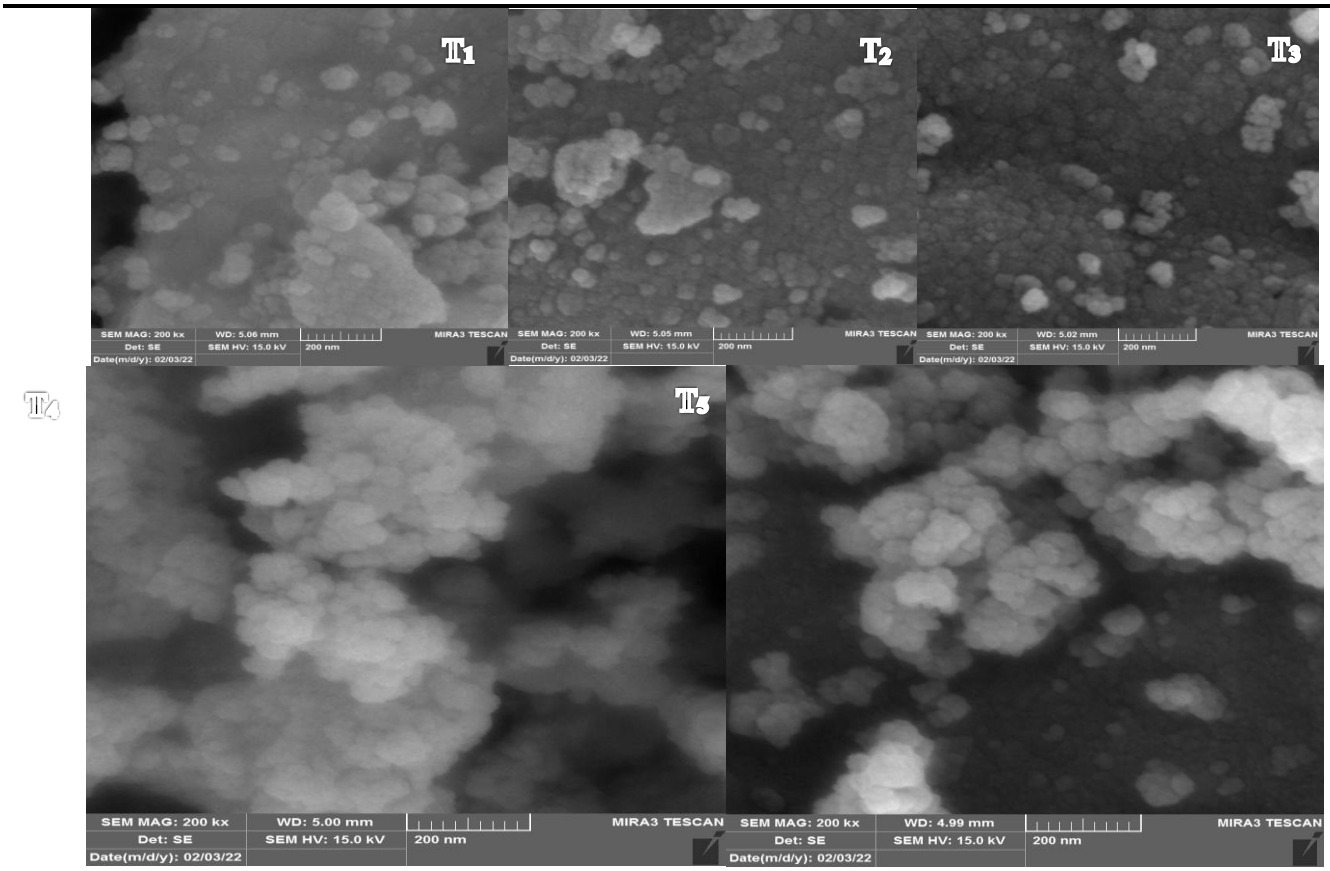

Figure (6): FE-SEM micrographs of (a) pure TiO_2, (b), (c), (d), and (e) are $Zn_{0.45}Mn_{0.55}Fe_2O_4$ mixed with different ratios of TiO_2 (20, 30, 40, and 50 %) respectively.

3.3 FT-IR spectrum of the Mn-Zn-ferrites and Mn-Zn-ferrites /TiO_2 nanocomposite

Figure 7 shows the FT-IR spectra of $Zn_{0.25}Mn_{0.75}Fe_2O_4$ ferrite nanocomposites. The asymmetric and symmetric C=O stretching modes are responsible for the bands at 1,516 and 1,600 cm-1, respectively, because metal ions coordinate the citric acid's carboxylate groups. The absorption peak at roughly 444, 567, and 665 cm^{-1} was clearly proven to be caused by the stretching of Fe–O, and Mn–O, ZnO bonds [25 - 26].

Analysis of the adsorbent's functional groups was carried out using the Fourier-transform infrared spectroscopy developed by BRUKER and the ALPHA model at a range of 400 to 3800 cm^{-1}. Because each band belongs to a distinct group, the functional groups and the numbers assigned to them can be determined, as illustrated in Figure 8 [27]. Figure 6 shows the FT-IR spectrum of pure TiO_2 nanoparticles and $Zn_{0.25}Mn_{0.75}Fe_2O_4$ mixed with different ratios (20, 30, 40, 50, and 60 %) of TiO_2 nanoparticles, which was calcined at 500 ^oC to study the produced $Zn_{0.25}Mn_{0.75}Fe_2O_4$ ferrite nanocomposite. The peak at 1641 cm^{-1}, 2344 cm^{-1} is indicative of the bands in the TiO_2 substance, whereas the peak at 500 cm^{-1} to 600 cm^{-1} is indicative of metal Fe-O, Mn-O and Zn-O bonds [28].

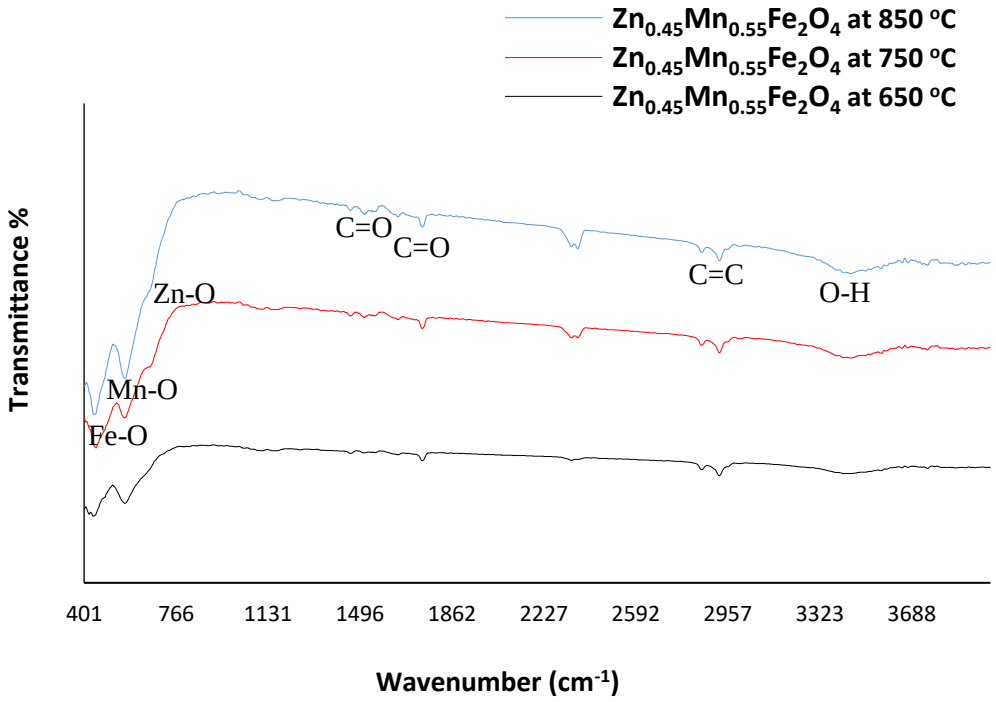

Figure (7): FT-IR spectrum of $Zn_{0.45}Mn_{0.55}Fe_2O_4$ ferrite nanocomposites at different calcination temperatures (650, 750, and 850 ˚C) by sol-gel method.

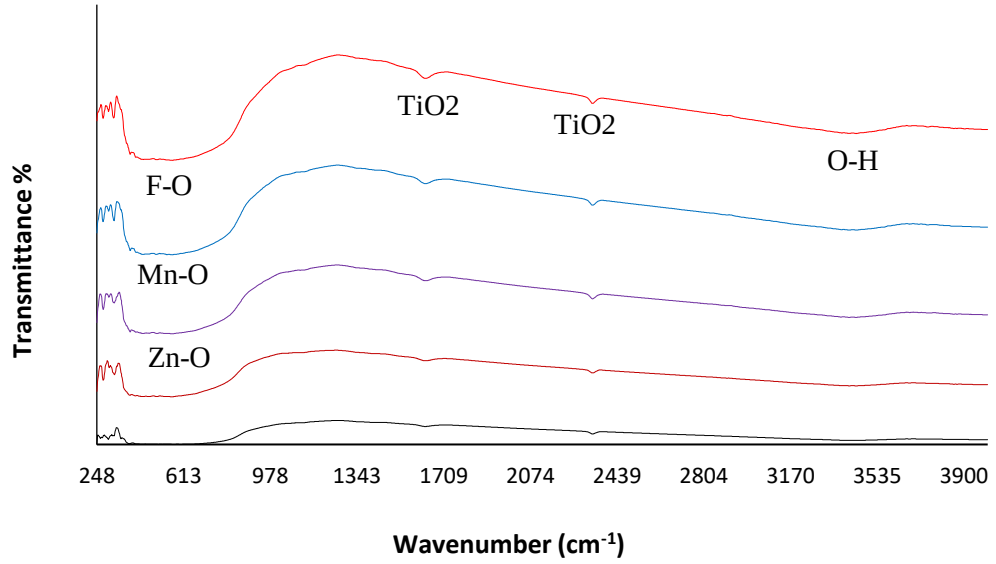

Figure (8): FTIR spectrum of (A) pure TiO_2, (B), (C), (D), (E) and (F) are $Zn_{0.45}Mn_{0.55}Fe_2O_4$ mixed with different ratios of TiO_2 (20, 30, 40, 50 and 60%) respectively.

4. Conclusion

Mn-Zn-Fe_2O_4 and $Zn_{0.45}Mn_{0.55}Fe_2O_4$ / TiO_2 NPs were successfully synthesized by a simple sol–gel method at 650, 750, and 850 °C. XRD results confirm pure cubic spinel crystalline structure for the sample. The average crystallite size was calculated by Debye-Scherrer formula. An examination into the possibility of producing the Mn-Zn-ferrites (NPs) by sol-gel and Mn-Zn-ferrites /TiO_2 (NC) as prospective structure-tunable nanomaterials is described in this report. X-ray diffraction (XRD), field emission-scanning electron microscopy (FE-SEM), and Fourier-transform infrared (FTIR) spectroscopy were used to characterize the structural properties of the Mn-Zn-ferrites by sol-gel and Mn-Zn-ferrites /TiO_2 (NC). They were 27 to 30 nm in

size with a cubic structure, while the Mn-Zn-ferrites /TiO_2 (NC) were 10 to 30 nm in size with a cubic structure. FE-SEM images showed the synthesized the Mn-Zn-ferrites and the Mn-Zn-ferrites /TiO_2 (NC) had a nanoparticle-like structure with a particle size of 27.77, to 72.04 nm. The strong FT-IR absorption peaks at 500 and 600 cm^{-1} represented an Fe-O, Mn-O, and Zn-O vibration band and 1667 cm^{-1} represented an TiO_2 for the Mn-Zn-ferrites and the Mn-Zn-ferrites /TiO_2 (NC), respectively.

References

1. Logeswari, P., Silambrasan, S., Jayanthi, A.: Synthesis of silver nanoparticles using plants extract and analysis of their antimicrobial property. J. Saudi Chem. Soc. **19**, 311–317 (2015)
2. Burda, C., Chen, X., Narayanan, R., El-Sayed, M.A.: Chemistry and properties of nano crystals of different shapes. Chem. Rev. **105**, 1025–1102 (2005).
3. Lin, X., Sun, M., Gao, B., Ding, W., Zhang, Z., Anandan, S., & Umar, A. (2021). Hydrothermally regulating phase composition of TiO2 nanocrystals toward high photocatalytic activity. *Journal of Alloys and Compounds*, *850*, 156653.
4. Thill, A., Zeyons, O., Spalla, O., Chauvat, F., Rose, J., Auffan, M.: Cytotoxicity of CeO_2 nanoparticles for *Escherichia coli*, physico-chemical insight of the cytotoxicity mechanism. Environ. Sci. Technol. **40**, 6151–6156 (2006).
5. Apperlot, G., Lipovsky, A., Dror, R., Perkas, N., Nitzan, Y., Lubart, R.: Enhanced anti bacterial activity of nanocrystalline ZnO due to increased ROS-mediated cell injury. Adv. Funct. Mater. **19**, 842–852 (2009)
6. Shankar, B., Krishnan, S., Vasantha, M., Arun, B., Williams, P.H.: Outer membrane proteins of wild-type and intimin-deficient enteropathogenic *Escherichia coli* induce Hep-2 cell death through intrinsic and extrinsic pathways of apoptosis. Int. J. Med. Microbiol. **299**, 121–132 (2009)
7. Giri, A., Goswami, N., Sasmal, C., Polley, N., Majumdar, D., Sarkar, S., Bandyopadhyay, S.N., Singha, A., Pal, S.K.: Unprecedented catalytic activity of Mn_3O_4 nanoparticles: potential lead of a sustainable therapeutic agent for hyperbilirubinemia. RSC Adv. **4**(10), 5075–5079 (2014)
8. Pal, M., Lee, S., Kwon, D., Hwang, J., Lee, H., Hwang, S., Jeon, S.: Direct immobilization of antibodies on Zn-doped Fe_3O_4 nanoclusters for detection of pathogenic bacteria. Anal. Chim. Acta **952**, 81–87 (2017)
9. Hastings, J.M., Corliss, L.M.: Neutron diffraction study of manganese ferrite. Phys. Rev. **104**, 328–331 (1956)
10. Elfalaky, A., Soliman, S.: Theoretical investigation of $MnFe_2O_4$. J. Alloys Compd. **580**, 401–406 (2013)
11. Li, J., Yuan, H., Li, G., Li, Y., Leng, J.: Cation distribution dependence of magnetic properties of sol–gel prepared $MnFe_2O_4$ spinel ferrite nanoparticles. J. Magn. Magn. Mater. **322**, 3396–3400 (2010)
12. Pradhan, P., Giri, J., Samanta, G., Sarma, H.D., Mishra, K.P., Bellare, J.R., Banerjee, R., Bahadur, D.: Comparative evaluation of heating ability and biocompatibility of different ferrite based magnetic fluids for hyperthermia application. J. Biomed. Mater. Res. B **81B**, 12–22 (2007)
13. Pal, M., Singh, A.K., Rakshit, R., Mandal, K.: Facile functionalization of Fe_2O_3 nanoparticles to induce inherent photoluminescence and excellent photocatalytic activity. Appl. Phys. Lett. **104**, 233110 (2014)
14. Pal, M., Kundu, A., Rakshit, R., Mandal, K.: Surface chemistry modulated introduction of multifunctionality within Co_3O_4 nanocubes. RSC Adv. **5**(21), 16311–16318 (2015)
15. Pal, M., Kundu, A., Rakshit, R., Mandal, K.: Ligand induced evolution of intrinsic fluorescence and catalytic activity from cobalt ferrite nanoparticles. Chem. Phys. Chem. **8**(16), 1627–1634 (2015)

16. Chen, D., Zhang, Y., Kang, Z.: A low temperature synthesis of $MnFe_2O_4$ nanocrystals by microwave-assisted ball-milling. Chem. Engg. J. **215**, 235–239 (2013)
17. Singh, M., Sud, S.P.: Controlling the properties of magnesium–manganese ferrites. Mater. Sci. Eng. B **83**, 180–184 (2001)
18. Lakshman, A., Rao, K.H., Mendiratta, R.G.: Magnetic properties of In^{3+} and Cr^{3+} substituted Mg–Mn ferrites. J. Magn. Magn. Mater. **250**, 93–97 (2002)
19. Wolski, W., Wolska, E., Kaczmarek, J., Piszora, P.: Formation of manganese ferrite by modified hydrothermal method. Phys. Status Solidi **152**, 19–22 (1995)
20. Pal, M., Rakshit, R., Mandal, K.: Surface modification of $MnFe_2O_4$ nanoparticles to impart intrinsic multiple fluorescence and novel photocatalytic properties. ACS Appl. Mater. Interfaces **6**(7), 4903–4910 (2014).
21. Abdullah, M. Z., Al-Timimi, M. H., Albanda, W. H., Dumitru, M., Balan, A. E., Ceaus, C., ... & Stamatin, I. (2019). STRUCTURAL AND ELECTROCHEMICAL PROPERTIES OF P3-Na0. 67Mn0. 3Co0. 7O2 NANOSTRUCTURES PREPARED BY CITRIC-UREA SELF-COMBUSTION ROUTE AS CATHODE FOR SODIUM ION BATTERY. DIGEST JOURNAL OF NANOMATERIALS AND BIOSTRUCTURES, 14(4), 1179-1193.
22. Rath, C., Anand, S., Das, R. P., Sahu, K. K., Kulkarni, S. D., Date, S. K., & Mishra, N. C. (2002). Dependence on cation distribution of particle size, lattice parameter, and magnetic properties in nanosize Mn–Zn ferrite. Journal of Applied Physics, 91(4), 2211-2215.
23. Varshney, D., Verma, K., & Kumar, A. (2011). Structural and vibrational properties of ZnxMn1− xFe2O4 (x= 0.0, 0.25, 0.50, 0.75, 1.0) mixed ferrites. Materials Chemistry and Physics, 131(1-2), 413-419.
24. S.J. Moeen, M.R. Vaezi, A.A. Yousefi, Prog. Color Colorants Coat. 3, 9 (2010).
25. S.K. Apte, S.D. Naik, R.S. Sonawane, B.B. Kale, J.O. Baeg, J. Am. Ceram. Soc. 90, 412 (2007).
26. Wang, K.; Jinwen, G.; Yin, N. Efficient Removal of Pb (II) and Cd (II) Using NH2-functionalized Zr-MOFs via Rapid Microwave-promoted Synthesis. Ind. Eng. Chem. Res. 2017, 56(7), 1880–1887. DOI: 10.1021/acs. iecr.6b04997.
27. Alamery, N.; Abid, H. R.; Wang, S. Adsorptive Study of Removing Harmful Dye (Methyl Orange) by Three Types of UiO-66 Metal Organic Framework. Chemeca. 2018, 2018, 156.
28. Nasehi, P., Abbaspour, S. F., Rafiee, M., & Moghaddam, M. S. (2021). Synthesis of novel acid-promoted UIO-66-NH2-MnFe2O4-TiO2-TiNT nanocomposite for high synchronous adsorption of cadmium and methyl orange and conditions optimization by response surface methodology. *Separation Science and Technology*, *56*(5), 884-902.
29. Cheng, S., Li, W., Xiao, S., Zheng, S., Chen, Z., Hu, L., ... & Chen, Q. (2021). Effects of calcination temperature on electrochemical properties of cathode material Na4MnV (PO4) 3/C synthesized by sol-gel method for sodium-ion batteries. *Journal of Alloys and Compounds*, *850*, 156707.